Absorption spectra of calix[3]pyrrole analogues as probes for contracted macrocycles

Keita Watanabe[a†], Ranajit Saha[b†], Yuya Inaba[a], Yumehiro Manabe[a], Tomoki Yoneda[a], Yuki Ide[b], Yuh Hijikata[b] and Yasuhide Inokuma[*a,b]

[a]*Division of Applied Chemistry, Faculty of Engineering, Hokkaido University, Kita 13 Nishi 8 Kita-ku, Sapporo, Hokkaido 060-8628, Japan*

[b]*Institute for Chemical Reaction Design and Discovery (WPI-ICReDD), Hokkaido University, Kita 21, Nishi 10, Kita-ku, Sapporo, Hokkaido, 001-0021, Japan.*

[†]*These authors contributed equally to this work.*

Received date (to be automatically inserted after your manuscript is submitted)
Accepted date (to be automatically inserted after your manuscript is accepted)

ABSTRACT: Calix[3]pyrrole and its furan derivatives exhibited bathochromically shifted lowest-energy electronic transition bands in their absorption spectra compared with their calix[4] and calix[6]pyrrole analogues, despite the repeating units are the same. We also observed fluorescence emission for calix[3]-type macrocycles. The Stokes shift of the furan/pyrrole hybrid macrocycles, calix[2]furan[1]pyrrole and calix[1]furan[2]pyrrole, substantially varied depending on the solvent polarity. Non-covalent interaction (NCI) plot analyses indicated enhanced interactions between neighboring aromatic rings in the calix[3]pyrrole macrocycle, whereas such interactions were weak in calix[4]pyrrole, in which the interchromophore distance is remarkably longer than in calix[3]pyrrole. Theoretical analyses indicated that the red-shifted, lowest-energy bands of calix[3]pyrrole correspond to HOMO–LUMO transitions, the energy gap of which was narrow compared with calix[4]pyrroles. The characteristic absorption bands for calix[3]pyrrole and its related macrocycles are useful as probes for distinguishing such macrocycles from higher calix[*n*]pyrrole ($n \geq 4$) analogues that exhibit almost identical absorption spectra.

KEYWORDS: Calixpyrrole, UV-vis absorption, strained macrocycle

*Correspondence to: Yasuhide Inokuma, Division of Applied Chemistry, Faculty of Engineering, Hokkaido University, Kita 13 Nishi 8 Kita-ku, Sapporo, Hokkaido 060-8628, Japan TEL: +81-(0)11-706-6556, FAX: +81-(0)11-706-6557, e-mail: inokuma@eng.hokudai.ac.jp.

INTRODUCTION

Since the discovery of subphthalocyanine in 1972 by Meller and Ossko [1], tripyrrolic macrocycles have attracted broad attention as ring-contracted congeners of porphyrins and phthalocyanines. As represented by the 14π-aromatic nature of subporphyrins [2–4] and subphthalocyanines [5–7], unique π-conjugated systems of tripyrrolic macrocycles are of substantial interest. Various derivatives including subporphyrazine [8], triphyrin(2.1.1) [9], subazaporphyrin [10], and core-modified triphyrins [11–13] have been synthesized to investigate their visible absorption/fluorescence, energy transfer, electron transfer, and nonlinear optical properties. Recently we synthesized a new member of the tripyrrolic macrocycle family, calix[3]pyrrole (**1**) [14], which has a contracted porphyrinogen-like ring system. Calix[3]pyrrole stores large ring strain energy that comes from deformation of the pyrrole units and *meso*-carbon atoms, and undergoes strain-induced ring expansion under acidic conditions, which rapidly yet quantitatively forms calix[6]pyrrole [14,15]. The strain-induced ring expansion has also been applied to regioselective synthesis of pyrrole/furan hybrid-type macrocycles such as calix[2]furan[4]pyrrole from calix[1]furan[2]pyrrole. Behind the unique reactivity, optical properties of calix[3]pyrrole and its furan derivatives have received less attention, because their π-conjugation is as small as pyrrole/furan monomers.

In contrast to the relationship between porphyrin and expanded porphyrins [16], calix[*n*]pyrroles ($n \geq 4$) are expected to exhibit almost identical absorption spectra independently of the number of repeating units [17,18]. However, pyrrole units in calix[3]pyrrole are in close proximity, which implies considerable perturbation on the π–π* transitions of the pyrrole units. This situation motivated us to investigate the optical properties of calix[3]pyrrole **(1)** and its furan-embedded analogues **2**–**4**. In this paper, we report that calix[3]pyrrole and related macrocycles exhibit characteristically red-shifted, lowest-energy absorption bands compared with their calix[4]- and calix[6]-analogues **5**–**9**. Fluorescence emission was also observed as mirror images of the lowest-energy absorption bands. Interestingly, the Stokes shifts of the pyrrole/furan hybrid macrocycles, calix[1]furan[2]pyrrole (**2**) and calix[2]furan[1]pyrrole (**3**), substantially increased as the polarity of the solvent increased. Lippert–Mataga plot analysis indicated polar excited states for these hybrid-type macrocycles. Analysis of the crystal structures showed remarkably smaller bond angles of C(α)–C(*meso*)–C(α') for calix[3]pyrrole analogues **1**–**4** compared with **5** and **8**, leading to shorted interchromophre distances of **1**–**4**. Such shorter interchromophore distances of **1** resulted in the enhanced non-covalent interactions visualized by NCI plot analysis. Theoretical calculations indicated that the lowest-energy transition band of calix[3]pyrrole **1** predominantly corresponded to the HOMO-to-LUMO transition and was smaller than that of calix[4]pyrrole **5**. These optical properties demonstrate a novel feature of contracted calix[3]pyrroles and are useful for distinguishing contracted calix[3]-type macrocycles from larger analogues by optical spectroscopy.

EXPERIMENTAL

Materials and Reagents

Calix[3]pyrrole (**1**) and its derivatives **2**–**4** in Chart 1 were synthesized from cyclic polyketone precursors in accordance with the literatures [14,15]. For comparison of optical spectra, calix[4]pyrrole (**5**) [19], calix[6]pyrrole (**8**) [20], and their furan-analogues **6** [21], **7**, and **9** [22] were prepared following the reported protocols. 2,5-Di-*tert*-butylpyrrole (**10**) [23] and

2,5-di-*tert*-butylfuran (**11**) [24] were also synthesized as control monomers. All of the solvents for optical measurements were purchased from WAKO Pure Chemical Industries Ltd. and used without further purification unless otherwise mentioned.

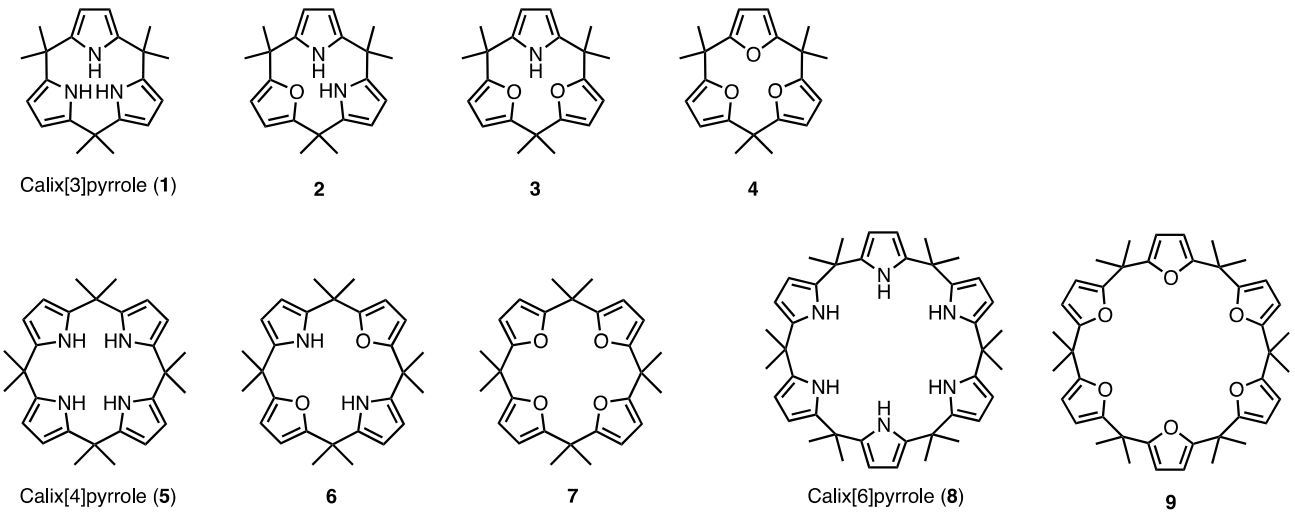

Chart 1. Structures of calix[3]pyrrole analogues **1**–**4** and larger derivatives **5**–**9**.

Instrumentation

UV/Vis absorption spectra were recorded on a Shimadzu UV-1800 spectrophotometer. Fluorescence spectra were recorded on a HITACHI F-7000 fluorescence spectrophotometer. Fluorescence quantum yields were measured by a Hamamatsu Photonics Quantaurus QY C11347-01.

Theoretical calculations

Theoretical calculations were performed with Gaussian 16 Rev. C01 [25]. Structures of the macrocycles were optimized at the B3LYP/cc-pVTZ level of theory with Grimme's D3BJ dispersion correction referring to their single crystal X-ray structures (CCDC deposition numbers: 2080605, 2127623, 2127624, and 2080606 for compounds **1**, **2**, **3**, and **4** respectively) as initial structures. Structure optimization of compound **5** (using the same calculation methods as for compounds **1**-**4**) was referred to the crystal structure (CCDC deposition number: 1288397) as the initial structure. The polarizable continuum model (IEFPCM) was also used to include the solvation effects of acetonitrile. Time-dependent density functional theory (TD-DFT) calculations were performed at the B3LYP/cc-pVTZ level of theory with Grimme's D3BJ dispersion correction. The polarizable continuum model (IEFPCM) was also used to include the solvation effects of acetonitrile. The NCI analysis was carried out based on the SCF approach [26–28] with NCIPLOT Version 4.0. [29]. The wavefunction files were generated at the B3LYP/aug-cc-pVTZ level of theory.

RESULTS AND DISCUSSION

Absorption and fluorescence spectroscopy

Calix[4]pyrrole (**5**) and calix[6]pyrrole (**8**) exhibited almost identical absorption spectra in acetonitrile, featuring π–π* transitions of pyrrole units at 225 and 231 nm, respectively (Fig. 1, left column). Compared with 2,5-di-*tert*-butylpyrrole (**10**) (Fig. S1), these absorption bands were slightly broadened, presumably because of weak interchromophore interactions of neighboring pyrrole units or the conformational flexibility of calix-type macrocycles. Interestingly, calix[3]pyrrole (**1**) exhibited a broad, red-shifted absorption band at 265 nm as well as strong absorption at 221 nm, in a similar manner to **5** and **8**. Upon photo-excitation at 250 nm, calix[3]pyrrole (**1**) emitted weak fluorescence at 340 nm (Φ_F = 0.02) as a mirror-image of the lowest-energy absorption band, whereas the fluorescence emission of **5** and **8** was too weak to be observed under the same measurement conditions.

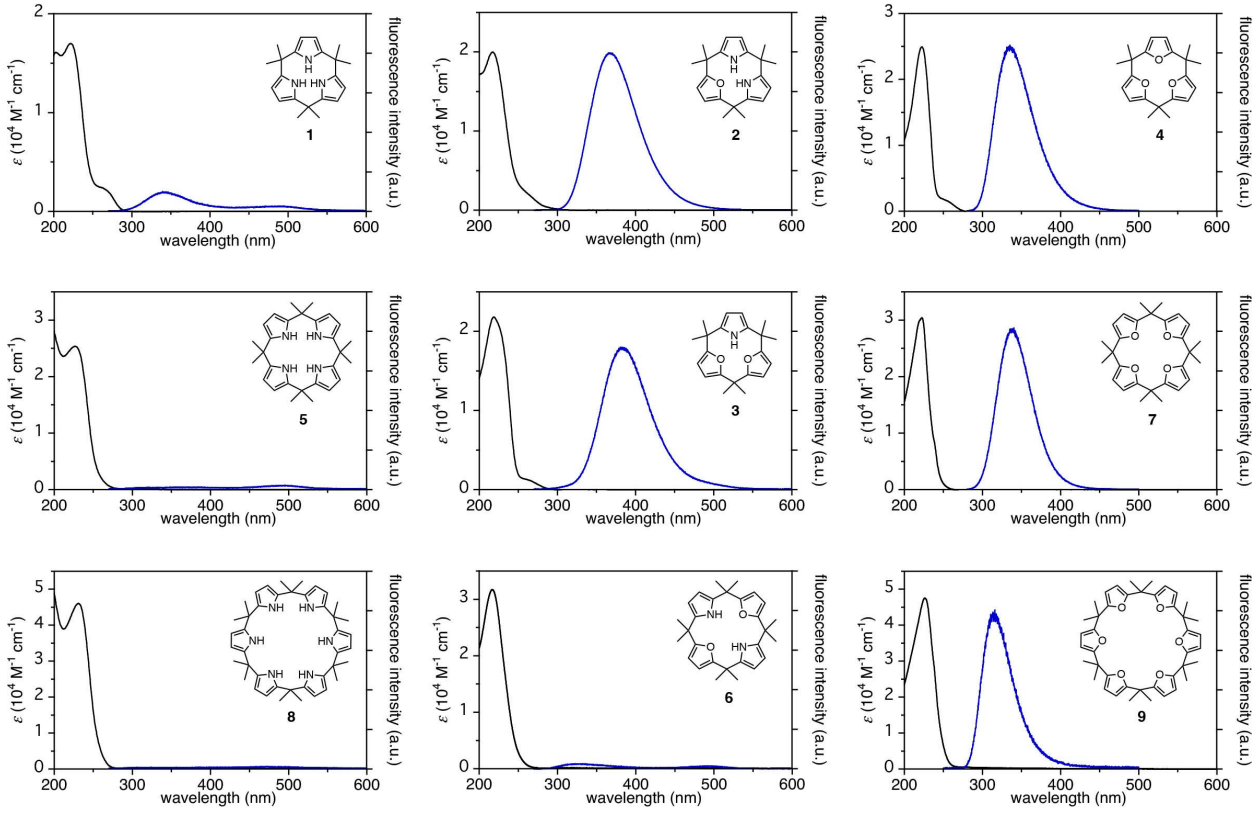

Fig. 1. Comparison of absorption (black lines) and fluorescence (blue lines) spectra of **1**–**9** in acetonitrile. (λ_{ex} = 250 nm for **1**–**6** and **8**, and 220 nm for **7** and **9**.)

Calix[*n*]furans **4** (*n* = 3), **7** (*n* = 4), and **9** (*n* = 6) also exhibited similar trends in their absorption spectra (Fig. 1, right column) to those of calix[*n*]pyrroles. Whereas the absorption spectra of **7** and **9** were virtually identical, only calix[3]furan (**4**) exhibited the broad lowest-energy transition band at 250 nm. Such broad transition bands were also observed for pyrrole/furan hybrid macrocycles **2** and **3** (Fig. 1, center column). Again, their calix[4]-type analogue **6** did not exhibit such

a broad band at 250–300 nm region. These results indicated that the weak and broad absorption bands at 250–300 nm are characteristic of calix[3]-type macrocycles. While **2** and **3** emitted fluorescence at 365 and 381 nm with quantum yields of Φ_F = 0.06 and 0.03, respectively, emission from calix[2]furan[2]pyrrole (**6**) was very weak.

Fluorescence emission of pyrrole/furan hybrid-type macrocycles **2** and **3** were largely affected by the solvent polarity. The emission peak wavelength of **2** was shifted from 342 nm (in *n*-hexane; Φ_F = 0.08) to 351 nm (1,4-dioxane; Φ_F = 0.04), 353 nm (ethanol; Φ_F = 0.03), 354 nm (tetrahydrofuran; Φ_F = 0.04), and 365 nm (acetonitrile; Φ_F = 0.06), while the absorption spectra in these solvents did not substantially shift. In a similar manner, the Stokes shift of compound **3** also changed from 372 nm (in *n*-hexane; Φ_F = 0.03) to 378 nm (1,4-dioxane; Φ_F = 0.03), 380 nm (ethanol; Φ_F = 0.03), 381 nm (tetrahydrofuran; Φ_F = 0.03), and 381 nm (acetonitrile; Φ_F = 0.03), although the amplitude of these changes was less than that of **2**.

To elucidate the solvent polarity dependence on the Stokes shift, we used Lippert–Mataga plot analysis [30] using the following equation, where the solvent polarity parameter Δf is expressed as a function of the dielectric constant ϵ_r and the refractive index n of the solvent:

$$\Delta f = \frac{\epsilon_r - 1}{2\epsilon_r + 1} - \frac{n^2 - 1}{2n^2 + 1}$$

When we plotted the Stokes shift (ΔE [cm^{-1}]) against the orientation polarizability (Δf), macrocycles **2** and **3** exhibited a larger slope than calix[3]pyrrole (**1**) and calix[3]furan (**4**) (Figs. 2 and S2), which indicated much polar excited states for furan/pyrrole hybrid systems **2** and **3**. Although macrocyclic π-conjugation is intercepted by *meso*-quaternary carbon atoms, the optical spectra of calix[3]pyrrole-related macrocycles suggested considerable interchromophore interaction, in particular among the furan and pyrrole units.

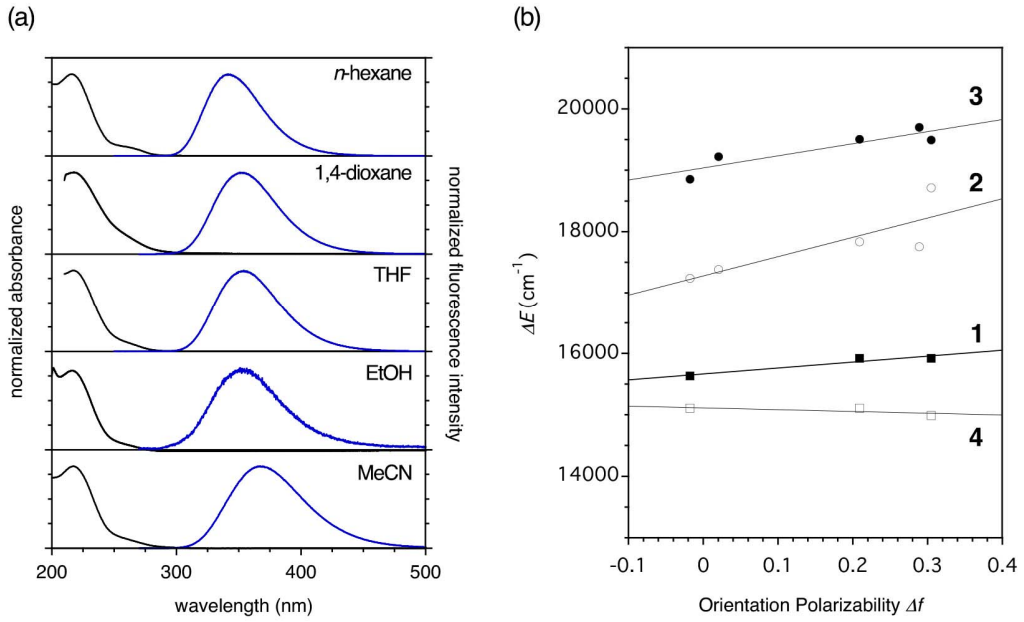

Fig. 2. Absorption (black lines) and fluorescence (blue lines) spectra of (a) **2** and (b) dependence between the Stokes shift (ΔE) and orientation polarizability (Δf) for **1**–**4**.

Comparison of molecular structures

The crystal structures of calix[*n*]pyrroles **1**, **5**, and **8** also exhibited structural differences in terms of the center-to-center distance between the pyrrole rings (Fig. S3a). The averaged bond angles of C(α)–C(*meso*)–C(α') for **1** was 106.2º (Fig. S3b), which was substantially smaller than those for **5** and **8** (109.7º and 111.3º, respectively). Such difference in the bond angles resulted in the close arrangement of the neighboring pyrrole units, namely, the averaged interchromophore distance (defined as the center-to-center distance of two neighboring aromatic units) was calculated to be 3.99, 4.35, and 4.42 Å for **1**, **5**, and **8**, respectively. We observed similar tendencies were also seen for furan-embedded macrocycles (Table 1). Although fast ring-flipping motion that changes the orientation of the aromatic rings occurs in solution even for calix[3]-type macrocycles [14], the close arrangement of the aromatic rings in calix[3]-type macrocycles **1**–**4** implies much stronger through-space interactions between neighboring arenes than larger analogues **5**–**9**.

Table 1. The C(α)–C(*meso*)–C(α') bond angles and interchromophore distances of **1**–**5**, and **8**.

Compound	**1**	**2**	**3**	**4**	**5**	**8**
C(α)–C(*meso*)–C(α') bond angle (º)	106.2	106.5	106.6	106.4	109.7	111.3
interchromophore distance (Å)	3.98	3.99	3.98	3.94	4.35	4.42

NCI plot analysis

To further investigate non-covalent interactions between the aromatic rings on calix[3]-type macrocycles **1**–**4**, we performed NCI plot analysis. The plot of s(*r*) against sign(λ_2)ρ(*r*) of **1** in Fig. 3 indicates that peaks appear within the range from –0.02 to 0.02, indicating that only van der Waals type interactions presented as non-covalent interactions. The plot of the isosurface of s(*r*) shows weak van der Waals interactions at the internal cavity of **1** among these pyrrole rings. Other calix[3]pyrrole analogues **2**–**4** also had van der Waals type weak interactions among the aromatic rings. Comparatively stronger NH•••O interactions for calix[2]furan[1]pyrrole (**3**) indicated hydrogen bonds in its bowl-like conformation, compared with that of calix[1]furan[2]pyrrole (**2**) (Fig. S4). When calix[4]pyrrole (**5**) was compared with **1** at the same threshold, the van der Waals type non-covalent interactions between neighboring pyrrole rings were negligible. These results also indicated that calix[3]-type macrocycles provide a platform in which non-covalent interactions among the aromatic units are enhanced. Despite the strained macrocyclic ring system, distinctly repulsive non-covalent interaction was not observed in the internal cavity for calix[3]pyrrole-related macrocycles **1**–**4**.

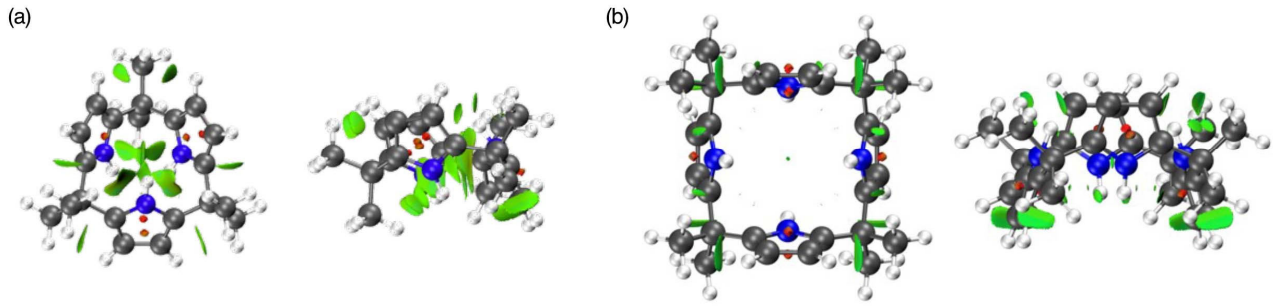

Fig. 3. The isosurface of s(r) = 0.5 mapped for (a) **1** and (b) **5** helped to inspect these interactions visually in the system. Left: viewed from top; and right: viewed from side. Color code: blue, green, and red isosurfaces indicate attractive, van der Waals type, and repulsive interactions, respectively.

Molecular orbital calculations

When frontier orbitals of calix[3]pyrrole (**1**) were compared with those of calix[4]pyrrole (**5**), stabilization of the lowest unoccupied π*-orbital of the pyrrole rings was characteristic for **1** (Fig. 4). The energy level of the lowest unoccupied π*-orbital for **1** was 0.64 eV lower than that of **5**. In contrast, the HOMO of **1** was slightly (0.07 eV) higher than that of **5**. As a result, the calculated lowest π-π* transition energy of **1** was 0.71 eV smaller than that of **5**. As observed for some cyclophanes [31–33], the narrowing HOMO–LUMO gap might be explained by the deformation of the aromatic units in **1**. TD-DFT calculations indicated that the lowest-energy transition of **1** (oscillator strength f = 0.0429) was mainly contributed by the HOMO-to-LUMO transition, which was assignable to the broad absorption band at 250–280 nm in Fig. 1. Theoretical calculations also indicated that the UV absorption spectra of calix[3]pyrrole (**1**) is characteristic of the strained macrocyclic ring system and can be used as a probe to distinguish from larger calix[n]pyrroles.

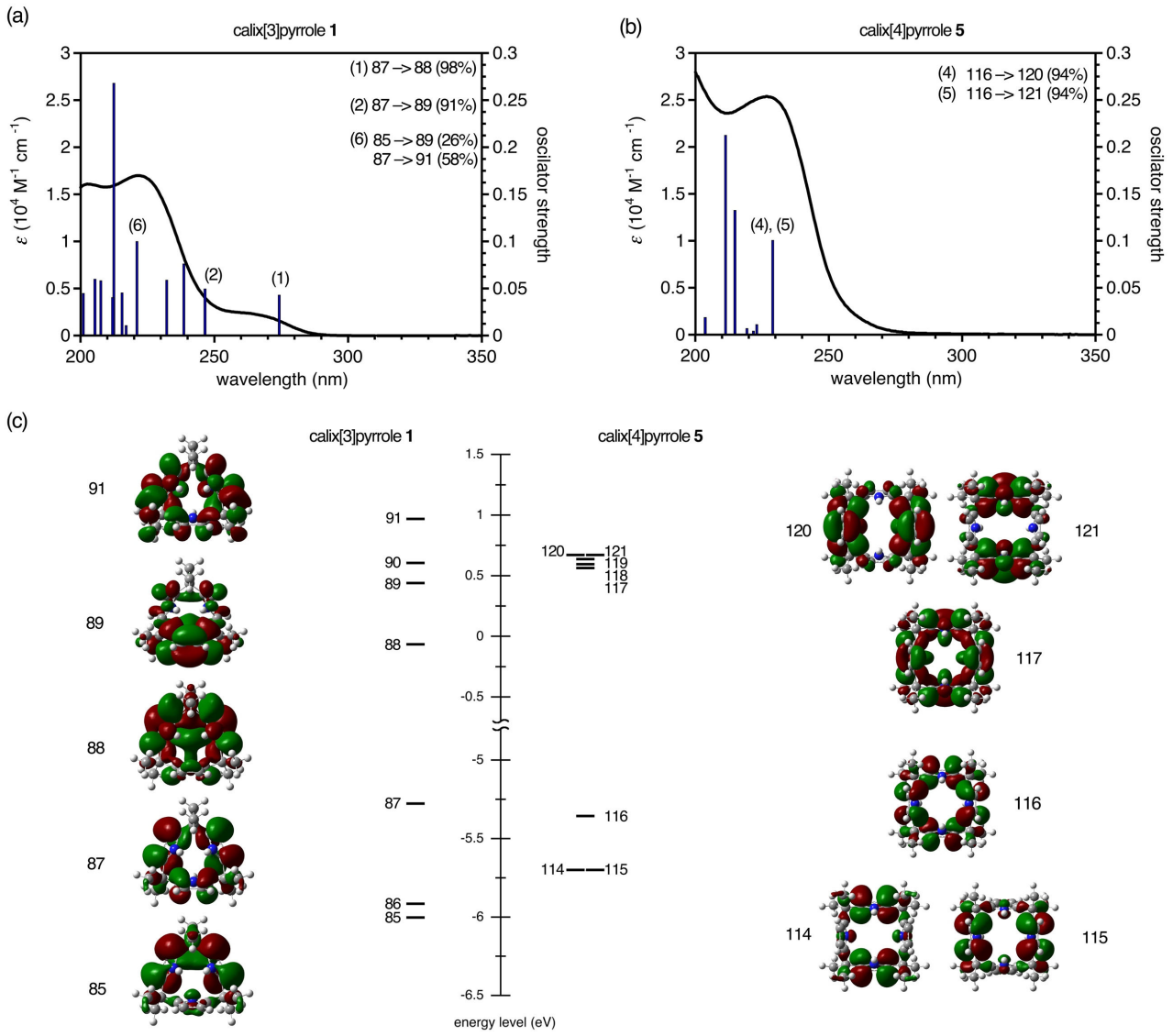

Fig. 4. (a, b) Experimental absorption spectra (black lines) and calculated electronic transitions (blue bars) for **1** and **5**, respectively. (c) Illustration of selected energy diagram and molecular orbitals for **1** and **5** related to their calculated electronic transitions.

CONCLUSIONS

In conclusion, we disclosed the optical absorption and fluorescence properties of calix[3]pyrrole (**1**) and its furan-embedded analogues **2**–**4**. The broad, red-shifted, lowest-energy bands around 250–300 nm were commonly observed for calix[3]-type macrocycles, but not for calix[4]- and [6]-pyrroles. Regarding pyrrole/furan hybrid-type macrocycles **2** and **3**, we observed the solvent polarity dependent Stokes shift changes, which indicated polar excited states. Theoretical calculations indicated that the calix[3]-type macrocycles had narrow HOMO–LUMO gaps as compared with calix[4]pyrrole analogues. These distinctive optical properties corresponded to the unique structures of calix[3]-type macrocycles; namely, deformation of the tripyrrolic links and close arrangement of the aromatic units. Although the absorption spectra of higher calix[*n*]pyrroles ($n \geq$

4) exhibited almost identical spectral pattern, the characteristically red-shifted lowest-energy bands of calix[3]pyrrole derivatives can be used as probes for distinguishing contracted macrocycle by UV-vis absorption spectroscopy.

Acknowledgements

This work was partly supported by a JSPS Grant-in-Aid for Challenging Research (Exploratory) (No. 20K21214), Scientific Research (B) (No. 22H0205802), and JST FOREST Program (No. PJ2522A005), of which Y. Inokuma is the principal investigator. The Institute for Chemical Reaction Design and Discovery (ICReDD) was established by World Premier International Research Initiative (WPI), MEXT, Japan. Y. Ide is grateful for a Grant-in-Aid for Early-Career Scientists grant (No. 21K14597) and Scientific Research on Innovative Areas “Soft Crystals”. Y.H. is grateful for a JSPS Grant-in-Aid for Challenging Research (Exploratory) (No. 21K18970). Y. Inaba would like to appreciate for the Grant-in-Aid for JSPS research fellow (No. 21J20973). Y.M. would also like to appreciate for the Grant-in-Aid for JSPS research fellow (No. 21J11228).

REFERENCES

1. Meller A, Ossko A. *Monatsh. Chem*. 1972; **103**: 150-155.
2. Inokuma Y, Kwon JH, Ahn TK, Yoo M-C, Kim D, Osuka A. *Angew. Chem. Int. Ed.* 2006; **45**: 961-964.
3. Shimizu S. *Chem. Rev.* 2017; **117**: 2730-2784.
4. Osuka A, Tsurumaki E, Tanaka T. *Bull. Chem. Soc. Jpn.* 2011; **84**: 679-697.
5. G. Claessens C, González-Rodríguez D, Torres T. *Chem. Rev*. 2002; **102**: 835-853.
6. Dowds M, Nielsen MB. *Mol. Syst. Des. Eng.* 2021, **6**, 6–24.
7. Claessens GC, Gonzáles-Rodríuez D, Iglesias SR, Torres T. *C. R. Chimie*. 2006; **9**: 1094-1099.
8. Rodríguez-Morgade M.S, Esperanza S, Torres T, Barberá J. *Chem. Eur. J.* 2005; **11**: 354-360.
9. Prasannan D, Ravikanth M. *Coord. Chem. Rev.* 2020; **407**: 213172.
10. Remiro-Buenamañana S, Díaz-Moscoso A, Hughes LD, Bochmann M, Tizzard JG, Coles JS, Cammidge NA. *Angew. Chem. Int. Ed*. 2015; **54**: 7510-7514.
11. Kuzuhara D, Sakakibara Y, Mori S, Okujima T, Uno H, Yamada H. *Angew. Chem. Int. Ed*. 2013; **53**: 3360-3363.
12. Pawlicki M, Garbicz M, Szterenberg L, Latos- Grażyński L. *Angew. Chem. Int. Ed*. 2015; **54**: 1906-1909.
13. Myśliborski R, Latos-Grażyński L, Szterenberg L, Lis T. *Angew. Chem. Int. Ed*. 2006; **45**: 3670-3674.
14. Inaba Y, Nomata Y, Ide Y, Pirillo J, Hijikata Y, Yoneda T, Osuka A, L. Sessler J, Inokuma Y. *J. Am Chem. Soc*. 2021; **143**: 12355-12360.
15. Inaba Y, Kakibayashi Y, Ide Y, Pirillo J, Hijikata Y, Yoneda T, Inokuma Y. *Chem. Eur. J*. 2022; **28**: e202200056.
16. Tanaka T, Osuka A. *Chem. Rev.* 2017; **117**: 2584–2640.
17. Liu K, Guo Y, Xu J, Shao JS, Jiang XS. *Chin. Chem. Lett.* 2006; **17**: 387-390.

18. Corsini A, Panoyan MJ. *J. Inorg. Nucl. Chem.* 1977; **39**: 1449-1450.
19. Rothemund P, Gage LC. *J. Am. Chem. Soc.* 1955; **77**: 3340-3342.
20. Cafeo G, Kohnke FH, La Torre GL, White AJP, Williams DJ. *Angew. Chem. Int. Ed.* 2000; **39**: 1496-1498.
21. Maupilier W, Journot G, Stoekli-Evans H, Neier R. *Eur. J. Org. Chem.* 2017: 6023-6037.
22. Healy SM, Rest AJ. *J. Chem. Soc., Perkin Trans, 1.* 1985: 973-982.
23. Licciulli S, Aldahiky K, Fomitcheva V, Korobkov I, Gambarottam Duchateau R. *Angew. Chem. Int. Ed.* 2011; **50**: 2346-2349.
24. Davis GA, Julia L, Yazdi NS. *J. Chem. Soc., Perkin Trans. 2* 1989: 239-244.
25. Gaussian 16, Revision C.01, Frisch, M. J.; Trucks, G. W.; Schlegel, H. B.; Scuseria, G. E.; Robb, M. A.; Cheeseman, J. R.; Scalmani, G.; Barone, V.; Petersson, G. A.; Nakatsuji, H.; Li, X.; Caricato, M.; Marenich, A. V.; Bloino, J.; Janesko, B. G.; Gomperts, R.; Mennucci, B.; Hratchian, H. P.; Ortiz, J. V.; Izmaylov, A. F.; Sonnenberg, J. L.; Williams-Young, D.; Ding, F.; Lipparini, F.; Egidi, F.; Goings, J.; Peng, B.; Petrone, A.; Henderson, T.; Ranasinghe, D.; Zakrzewski, V. G.; Gao, J.; Rega, N.; Zheng, G.; Liang, W.; Hada, M.; Ehara, M.; Toyota, K.; Fukuda, R.; Hasegawa, J.; Ishida, M.; Nakajima, T.; Honda, Y.; Kitao, O.; Nakai, H.; Vreven, T.; Throssell, K.; Montgomery, J. A., Jr.; Peralta, J. E.; Ogliaro, F.; Bearpark, M. J.; Heyd, J. J.; Brothers, E. N.; Kudin, K. N.; Staroverov, V. N.; Keith, T. A.; Kobayashi, R.; Normand, J.; Raghavachari, K.; Rendell, A. P.; Burant, J. C.; Iyengar, S. S.; Tomasi, J.; Cossi, M.; Millam, J. M.; Klene, M.; Adamo, C.; Cammi, R.; Ochterski, J. W.; Martin, R. L.; Morokuma, K.; Farkas, O.; Foresman, J. B.; Fox, D. J. Gaussian, Inc., Wallingford CT, 2016.
26. Johnson RE, Keinan S, Mori-Sánchez P, Contreras-García J, Cohen JA, Yang W. *J. Am. Chem. Soc.* 2010; **132**: 6498-6506.
27. Contreras-García J, Johnson RE, Keinan S, Chaudret R, Piquemal J-P, Baratan ND, Yang W. *J. Chem. Theory Comput.* 2011; **7**: 625-632.
28. Boto AR, Peccati F, Laplaza R, Quan C, Carbone A, Piquemal J-P, Maday Y, Contreras-García J. *J. Chem. Theory Comput.* 2020; **16**: 4150-4158.
29. Boto AR, Peccati F, Laplaza R, Quan C, Carbone A, Piquemal J-P, Maday Y, Contreras-Garcia J. NCIPLOT4: A new step towards a fast quantification of noncovalent interactions, https://github.com/juliacontrerasgarcia/nciplot, last accessed: 11th September 2022.
30. Mataga N, Kaifu Y, Koizumi M. *Bull. Chem. Soc.* 1956; **29**: 465-470.
31. Tsuji T, Ohkita M, Konno T, Nishida S. *J. Am. Chem. Soc.* 1997; **119**: 8425-8431.
32. Hermann M, Wassy D, Kratzert D, Esser B. *Chem. Eur. J.* 2018; **24**: 7374-7387.
33. Biswas S, Qiu SC, Dawe NL, Zhao Y, Bodwell JG. *Angew. Chem. Int. Ed.* 2019; **58**: 9166-9170.

Absorption spectra of calix[3]pyrrole analogues as probes for contracted macrocycles

Keita Watanabe, Ranajit Saha, Yuya Inaba, Yumehiro Manabe, Tomoki Yoneda, Yuki Ide, Yuh Hijikata and Yasuhide Inokuma*

Calix[3]pyrrole and its furan derivatives exhibited red-shifted electronic transition bands as compared with larger calix[4] and calix[6]pyrrole-type macrocycles, despite the repeating units are the same. Theoretical analyses indicated that the red-shifted, lowest-energy bands of calix[3]pyrrole analogues correspond to HOMO–LUMO transitions, the energy gap of which was narrow compared with calix[4]pyrroles. The characteristic absorption bands for calix[3]pyrrole and its related macrocycles are useful as probes for distinguishing such macrocycles from higher calix[*n*]pyrrole analogues that exhibit almost identical absorption spectra.